

To appear on the Proceedings of the 13th ICATPP Conference on  
Astroparticle, Particle, Space Physics and Detectors  
for Physics Applications,  
Villa Olmo (Como, Italy), 3–7 October, 2011,  
to be published by World Scientific (Singapore).

## ELECTRICAL CHARACTERIZATION OF SiPM AS A FUNCTION OF TEST FREQUENCY AND TEMPERATURE

M.J. Boschini<sup>1,3</sup>, C. Consolandi<sup>1</sup>, P.G. Fallica<sup>4</sup>, M. Gervasi<sup>1,2</sup>, D. Grandi<sup>1</sup>,  
M. Mazzillo<sup>4</sup>, S. Pensotti<sup>1,2</sup>, P.G. Rancoita<sup>1</sup>, D. Sanfilippo<sup>4</sup>,  
M. Tacconi<sup>1\*</sup> and G. Valvo<sup>4</sup>

<sup>1</sup>*Istituto Nazionale di Fisica Nucleare, INFN Milano-Bicocca, Milano (Italy)*

<sup>2</sup>*Department of Physics, University of Milano Bicocca, Milano (Italy)*

<sup>3</sup>*CILEA, Segrate (MI) (Italy)*

<sup>4</sup>*STMicroelectronics, Catania (Italy)*

*E-mail: mauro.tacconi@mib.infn.it*

Silicon Photomultipliers (SiPM) represent a promising alternative to classical photomultipliers for the detection of photons in high energy physics and medical physics, for instance. In the present work, electrical characterizations of test devices - manufactured by STMicroelectronics - are presented. SiPMs with an area of  $3.5 \times 3.5 \text{ mm}^2$  and a cell pitch of  $54 \mu\text{m}$  were manufactured as arrays of  $64 \times 64$  cells and exhibiting a fill factor of 31%. The capacitance of SiPMs was measured as a function of reverse bias voltage at frequencies ranging from about 20 Hz up to 1 MHz and temperatures from 310 K down to 100 K. Leakage currents were measured at temperatures from 410 K down to 100 K. Thus, the threshold voltage - i.e., the voltage above a SiPM begins to operate in Geiger mode - could be determined as a function of temperature. Finally, an electrical model capable of reproducing the frequency dependence of the device admittance is presented.

### 1. Introduction

In recent years Silicon Photomultipliers (SiPM) has been developed for usage in photon detection. The high gain, insensitivity to magnetic field and low reverse bias voltage of operation make SiPM a promising candidates as replacement of classical photomultipliers<sup>1</sup> in several of their applications. The SiPM is an array of parallel-connected single photon avalanche diodes (SPAD)<sup>2</sup>. Every SPAD operates in Geiger mode with a quenching resistor in series to prevent an avalanche multiplication process from taking place. The overall output of a SiPM depends on how many SPADs are

simultaneously ignited<sup>3,4</sup>.

The current SiPM device was manufactured by STMicroelectronics (details of the technology can be found in Refs.<sup>2,5</sup>). It consisted of an array of  $64 \times 64$  SPAD cells with  $3.5 \times 3.5 \text{ mm}^2$  effective area, a cell pitch of  $54 \mu\text{m}$  and a fill factor of  $\approx 31\%$ .

In the present article, the electrical characteristics of these devices are shown as function of test frequency from 1 MHz down to about 20 Hz and temperature from 410 K down to 100 K (Sects. 2–2.2). In addition, in Sects. 3 and 3.1 an electrical model is discussed and compared with data obtained from dependencies of capacitance and resistance on the test frequency for both a photodiode and a SiPM devices.

## 2. Electrical Characteristics of SiPM Devices

The electrical characteristics of SiPM devices were investigated as function of applied reverse bias voltage ( $V_r$ ) and temperature. The capacitance response was also studied as a function of test frequency of the capacitance meter employed for such a measurement (Sect. 2.1).

Furthermore (Sect. 2.2), the measurements of the SiPM leakage current allowed one to determine (as a function of temperature) the value (and its temperature dependence) of the so-called *threshold voltage* ( $V_{th}$ ), i.e., the

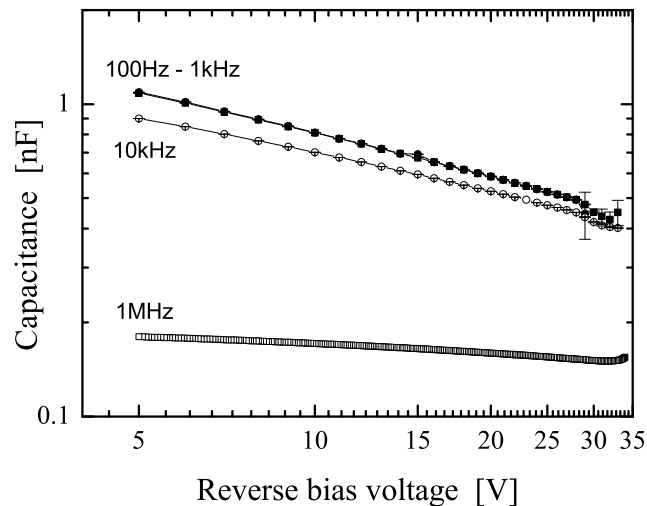


Fig. 1. Capacitance (in nF) as a function of reversed bias voltage (in V) using the LCZ meter with test frequencies of 100 Hz ( $\bullet$ ), 1 kHz ( $\blacksquare$ ), 10 kHz ( $\circ$ ) and BC with 1 MHz ( $\square$ ).

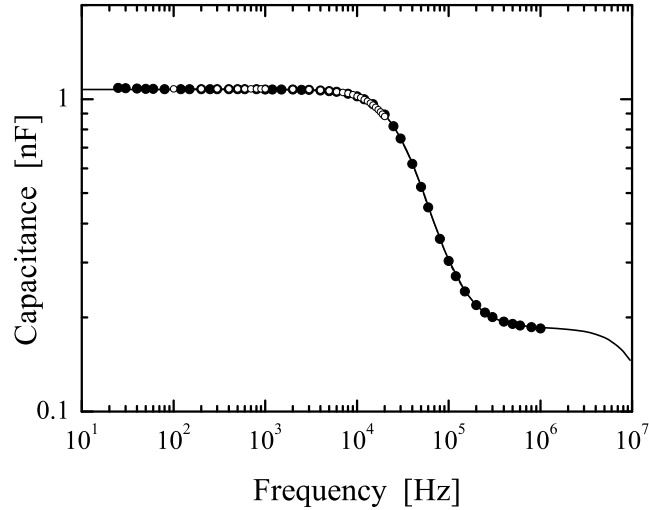


Fig. 2. Capacitance (in nF) as a function of the frequency (in Hz) for a sample operated with a reverse bias of 5 V: data points indicated with  $\bullet$  ( $\circ$ ) were obtained using the LCR (LCZ) meter, the continuous line is obtained from Eq. (9) (see discussion in Sect. 3.1).

reverse bias voltage above which a SiPM begins to operate in Geiger mode.

### 2.1. Capacitance Response

The capacitance response of SiPM devices was systematically measured as a function of reverse bias voltage applied and test frequency at 300 K (i.e., at room temperature). Moreover, using a liquid nitrogen cryostat, at a few fixed frequencies the capacitance was also measured as a function of reverse bias voltage and temperature from 310 K down to 100 K. For these purposes three instruments were employed, i.e., a Boonton capacimeter (BC) (using its internally provided power source and a test frequency of 1 MHz), an LCZ (Agilent Technologies 4276A) and LCR (Agilent Technologies 4284A) meters with the reverse bias supplied to the device from an external power supply. The LCZ meter employed test frequencies from 100 Hz up to 20 KHz; the LCR meter from  $\approx 20$  Hz up to 1 MHz. Furthermore, the measurements were performed selecting the parallel equivalent-circuit mode of the LCR and LCZ meters for the device under test (DUT). Thus, the device response is assumed to be that one from a parallel capacitor-resistor circuit (see discussion in Sect. 3). Finally, the currently reported experimental errors

4

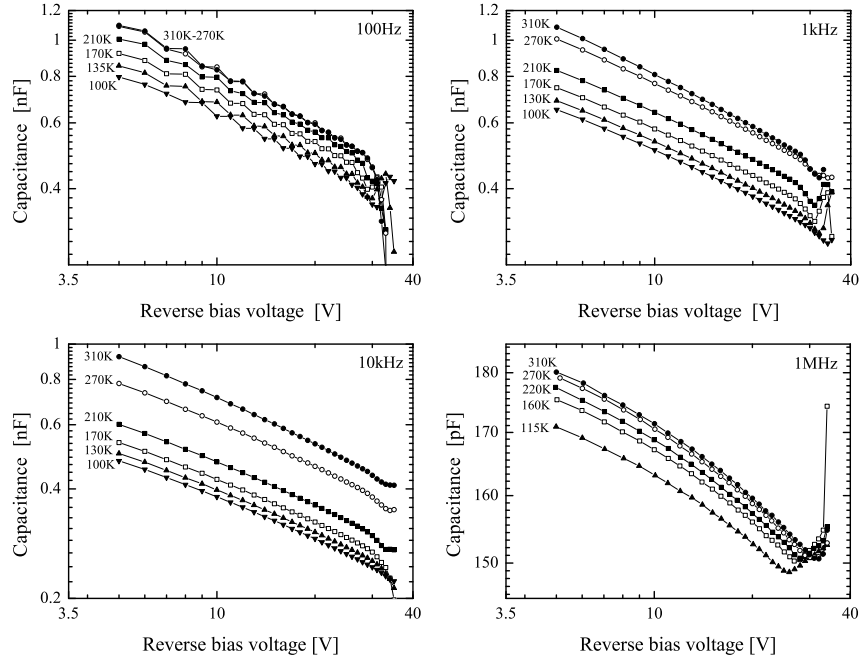


Fig. 3. Capacitance response (in nF or pF) obtained using the LCZ meter as a function of reverse bias applied (in V) and temperature from 310 K down to 100 K: 100 Hz (upper left), 1 kHz (upper right), 10 kHz (bottom left) and - using the BC - 1 MHz (bottom right).

are the standard deviations obtained using 50 subsequent measurements of the device capacitance under the same experimental conditions.

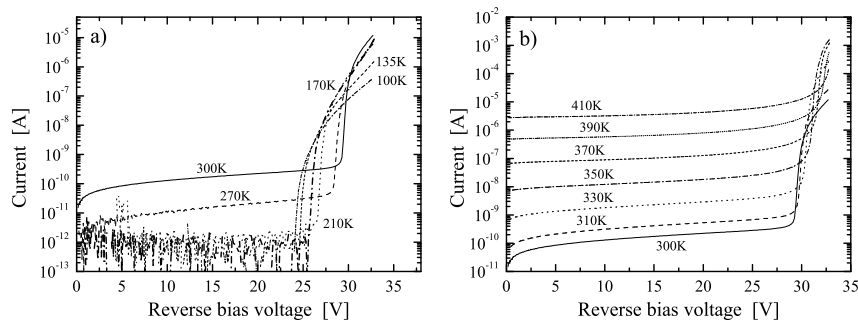


Fig. 4. (a) Leakage current (in A) as a function of reverse bias voltage (in V) from 310 down to 100 K; (b) leakage current (in A) as a function of reverse bias voltage (in V) from 300 up to 410 K.

In Fig. 1, the capacitance response of a SiPM using frequencies of 100 Hz, 1 kHz, 10 kHz and 1 MHz is shown as a function of  $V_r$  at 300 K. Above 1 kHz, the measured capacitance decreases with the increase of the test frequency. In Fig. 2, the capacitance response - determined using both LCZ and LCR meters - is shown for a device operated with a reverse bias voltage of 5 V at 300 K. It can be observed that above  $\approx 10$  kHz the measured capacitance largely decreases with the increase of the test frequency of the instrument up to achieving an almost constant response above a few hundreds of kHz.

In Fig. 3, the capacitance response using 100 Hz, 1 kHz, 10 kHz and 1 MHz is shown as a function of  $V_r$  (in V) and temperature from 310 K down to 100 K. The measured capacitance is observed to decrease with decreasing temperature. This behavior is also observed for frequencies lower than  $\approx 10$  kHz; while a similar capacitance response was exhibited at 300 K (see Fig. 1).

## 2.2. Current-Voltage Characteristics

The dependence of leakage current on reverse bias was studied as a function of temperature from 410 K down to 100 K as shown in Fig. 4. With increasing  $V_r$  the leakage current does not vary by more than an order of magnitude until the multiplication regime is ignited, i.e., so far the *threshold voltage*,  $V_{th}$ , is reached.  $V_{th}$  is the voltage corresponding to the value of leakage current at the intercept between the two  $I$  versus  $V$  curves obtained, the first when the multiplication regime is sharply starting and the second one at lower voltages, i.e., before the multiplication occurs: an example regarding the determination of the value of  $V_{th}$  at 270 K is reported in Fig. 5(a). As

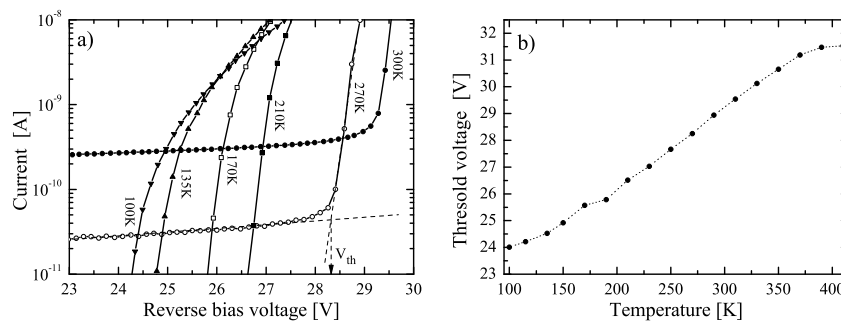


Fig. 5. (a) Leakage current (in A) as a function of reverse bias voltage applied (in V) and an example of threshold voltage,  $V_{th}$  in V, determination at 270 K; (b) threshold voltage (in V) as a function of temperature (in K).

6

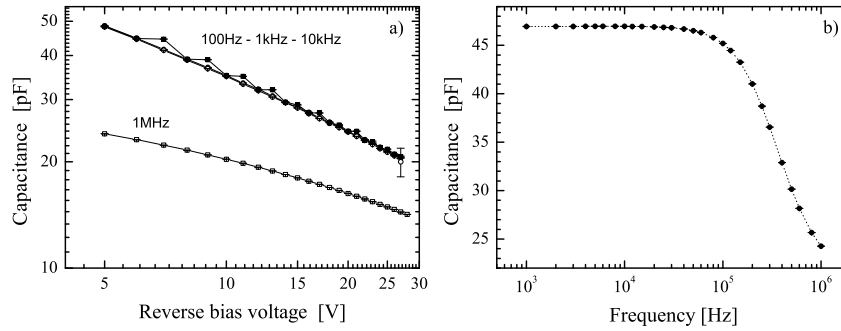


Fig. 6. (a) Capacitance (in pF) of a photodiode as a function of reverse bias voltage (in V) at 100 Hz, 1 kHz, 10 kHz (using the LCZ meter) and 1 MHz (using the BC); (b) capacitance (in pF) of a photodiode as a function of test frequency in Hz (using the LCR meter) with an applied reverse biased voltage of 6 V.

shown in Fig. 5(b), the threshold voltage lowers - thus, SPADs turn into a Geiger-mode regime at progressively lower reverse bias voltages - with lowering temperature at the rate of  $\approx -29$  mV/K from  $\approx 360$  down to  $\approx 130$  K.

### 3. Electrical Model

At room temperature, the electrical frequency response of SiPMs was further investigated using a test device manufactured by STMicroelectronics. The latter device was a photodiode (PD) with a structure similar to that of a SPAD cell, an active area of  $\approx 0.2$  mm<sup>2</sup>, but no quenching resistor in series. In Fig. 6(a), the capacitance of the PD is shown as a function of reverse bias voltage at 100 Hz, 1 kHz, 10 kHz and 1 MHz. Furthermore, one can see that the device exhibits almost no dependence on the test frequency below  $\approx 100$  kHz [Fig. 6(b)].

For silicon photodiodes and radiation detectors, the electrical response down to cryogenics temperatures is usually modeled using the so-called

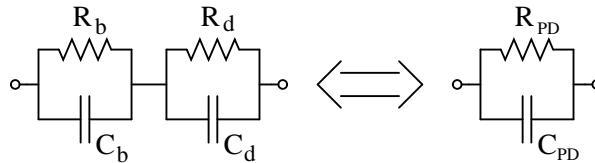


Fig. 7. SIJD model for silicon photodiodes and radiation detectors:  $C_d$  ( $C_b$ ) and  $R_d$  ( $R_b$ ) are the capacitance and resistance of the depleted (field free) region, respectively;  $C_{PD}$  and  $R_{PD}$  are the overall capacitance and resistance of the photodiode, respectively.

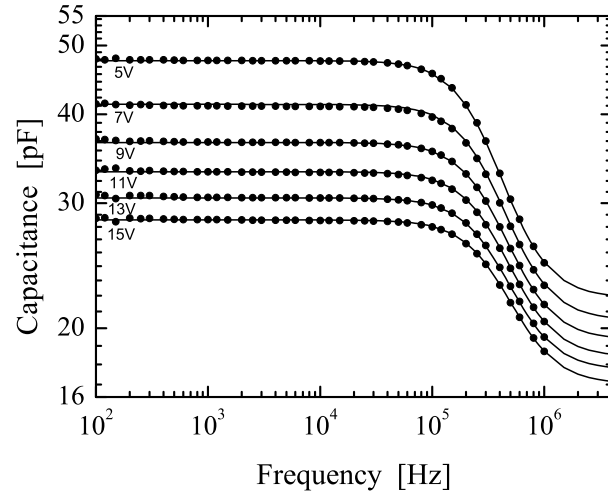


Fig. 8. Measured capacitance ( $\bullet$ ),  $C_{PD}$ , (in pF) as a function of test frequency (in Hz) with superimposed continuous lines obtained from the SIJD model [Eq. (3)].

*small-signal ac impedance of junction diode* (SIJD) operated under reverse bias (e.g., see Refs.<sup>6,7</sup>, Section 4.3.4 of Ref.<sup>8</sup> and references therein). In the framework of the SIJD model, the device consists of the depleted and field

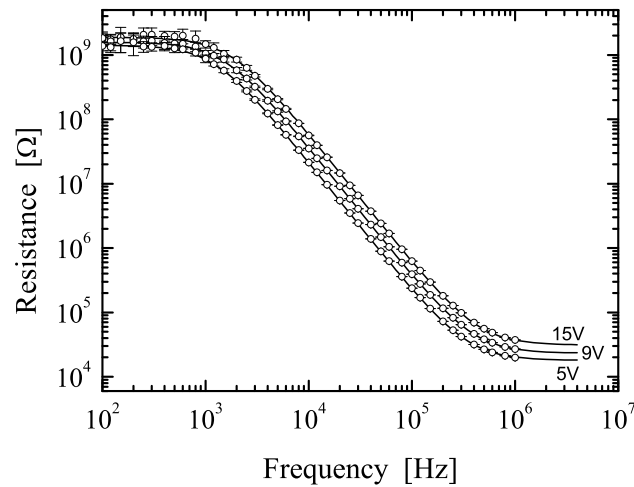


Fig. 9. Measured resistance ( $\circ$ ),  $R_{PD}$ , (in  $\Omega$ ) as a function of test frequency (in Hz) at 5, 9 and 15 V with superimposed continuous lines obtained from the SIJD model [Eq. (2)].

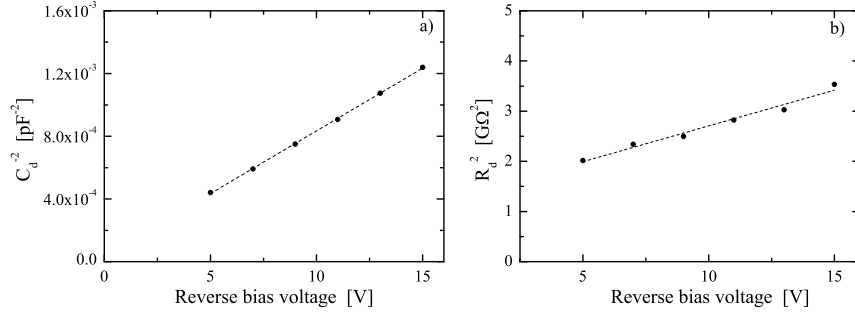


Fig. 10. (a)  $1/C_d^2$  (in  $\text{pF}^{-2}$ ) and (b)  $R_d^2$  (in  $\text{G}\Omega^2$ ) from Table 1 as a function of applied reversed bias voltage in V. The dashed lines are those from a linear fit to the data.

free regions connected in series. Each one of these regions, in turn, consists of a parallel-connected capacitor and resistor. In Fig. 7, the equivalent circuit of a photodiode is shown:  $C_d$  ( $C_b$ ) and  $R_d$  ( $R_b$ ) are the capacitance and resistance of the depleted (field free) region, respectively.

Labeling (Fig. 7) the overall<sup>§</sup> capacitance and resistance of a photodiode with  $C_{PD}$  and  $R_{PD}$ , respectively, one can express the admittance of the device as:

$$\begin{aligned} Y_{PD}(\omega) &= G_{PD}(\omega) + j B_{PD}(\omega) \\ &= \frac{1}{R_{PD}} + j \omega C_{PD} \end{aligned} \quad (1)$$

with  $\omega = 2\pi f$ , where  $f$  is the test frequency. The conductance (i.e., the real part of the admittance) and susceptance (the imaginary part of the admittance) are respectively given by:

$$G_{PD}(\omega) = \frac{1}{R_{PD}} = \frac{R_d + R_b + \omega^2 R_d R_b (R_d C_d^2 + R_b C_b^2)}{(R_d + R_b)^2 + \omega^2 R_d^2 R_b^2 (C_b + C_d)^2} \quad (2)$$

$$B_{PD}(\omega) = \omega C_{PD} = \omega \left[ \frac{\omega^2 R_d^2 R_b^2 C_d C_b (C_b + C_d) + R_d^2 C_d + R_b^2 C_b}{(R_d + R_b)^2 + \omega^2 R_d^2 R_b^2 (C_b + C_d)^2} \right] \quad (3)$$

[e.g., see Equations (4.184, 4.185) at page 455 of Ref.<sup>8</sup>].

It has to be remarked that the values of both  $C_{PD}$  and  $R_{PD}$  are those which can be determined, for instance, selecting the parallel equivalent-circuit mode for the DUT using the LCR meter. In the SIJD model, the values of  $C_d$ ,  $R_d$ ,  $C_b$  and  $R_b$  do not depend on the test frequency. In

<sup>§</sup> $C_{PD}$  and  $R_{PD}$  are the quantities directly measured selecting the parallel equivalent-circuit mode of the LCR and LCZ meters.



Table 1.  $C_d$ ,  $R_d$ ,  $C_b$  and  $R_b$  obtained from a fit of the SIJD model for a photodiode to experimental data as a function of reverse bias voltage ( $V_r$ ).

$V_r$ [V]	$C_d$ [pF]	$R_d$ [G $\Omega$ ]	$C_b$ [pF]	$R_b$ [k $\Omega$ ]
5	47.6	1.42	41.1	5.2
7	41.1	1.53	40.8	5.2
9	36.5	1.58	40.8	5.2
11	33.2	1.68	40.4	5.2
13	30.5	1.74	40.9	5.3
15	28.4	1.88	40.5	5.3

addition,  $C_d$ ,  $R_d$  are expected to depend on the applied reverse bias voltage, because the depleted layer width increases with increasing  $V_r$ .

$C_d$ ,  $R_d$ ,  $C_b$  and  $R_b$  were determined (Table 1) as a function  $V_r$ , by a fit to the measured quantities  $C_{PD}$  and  $R_{PD}$  (obtained using the LCR meter) using the corresponding expressions [e.g., see Eqs. (2, 3)] obtained from the SIJD model for a photodiode. For instance, in Fig. 8 (Fig. 9) the experimental data and fitted curves are shown for the capacitance (resistance) measurements as a function of test frequency and applied reverse bias voltage. As expected<sup>6</sup> (Table 1), the field free region is almost independent of  $V_r$ , while both the capacitance and resistance of the depleted region exhibit a dependence on the reverse bias. In Fig. 10,  $1/C_d^2$  [Fig. 10(a)] and  $R_d^2$  [Fig. 10(b)] values from Table 1 are shown as a function of applied reverse voltage. Although the junction photodiode cannot be considered as a one-sided step junction<sup>¶</sup>, the the dashed curves (Fig. 10) obtained from fits to the reported data - assuming a linear dependence of  $1/C_d^2$  and  $R_d^2$  on  $V_r$  - are well suited for reproducing the dependence on the reverse bias voltage.

### 3.1. Electrical Model for SiPMs

A SiPM device consists of a set of SPAD devices (4096 in the current SiPM under test) connected in parallel. The equivalent electrical circuit of the elemental cell (i.e., a SPAD cell) is shown in Fig. 11 and differs from that of a photodiode (discussed in Sect. 3) by a resistance ( $R_s$ ) added in series. In Fig. 11,  $C_d$  ( $C_b$ ) and  $R_d$  ( $R_b$ ) are the capacitance and resistance of the depleted (field free) region of the photodiode, respectively. In the present

<sup>¶</sup>The depletion layer characteristics as a function of reverse bias voltage can be found treated, for instance, in Chapter 6-2 of Ref.<sup>10</sup> (see also Ref.<sup>9</sup>).

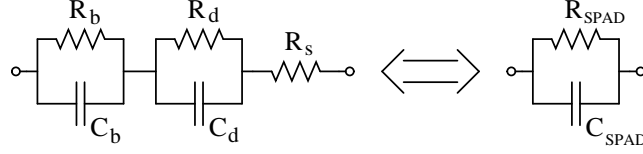


Fig. 11. SIJD model for a SPAD cell:  $C_d$  ( $C_b$ ) and  $R_d$  ( $R_b$ ) are, respectively, the capacitance and resistance of the depleted (field free) region with a series resistance  $R_s$ ;  $C_{\text{spad}}$  and  $R_{\text{spad}}$  are the overall capacitance and resistance of a SPAD cell, respectively.

technology of STMicroelectronics,  $R_s$  is typically about (0.2–1.0) M $\Omega$ .

The admittance ( $Y_{\text{spad}}$ ) of a SPAD cell is given by

$$\begin{aligned} Y_{\text{spad}}(\omega) &= G_{\text{spad}}(\omega) + j B_{\text{spad}}(\omega) \\ &= \frac{1}{R_{\text{spad}}} + j \omega C_{\text{spad}} \end{aligned} \quad (4)$$

with  $C_{\text{spad}}$  and  $R_{\text{spad}}$  respectively expressed in terms of  $C_d$ ,  $C_b$ ,  $R_d$ ,  $R_b$  and  $R_s$  as

$$\begin{aligned} C_{\text{spad}} &= \frac{B_{\text{spad}}(\omega)}{\omega} \\ &= \frac{\omega^2 R_d^2 R_b^2 C_d C_b (C_b + C_d) + R_d^2 C_d + R_b^2 C_b}{D_1 + D_2}, \end{aligned} \quad (5)$$

$$\begin{aligned} R_{\text{spad}} &= \frac{1}{G_{\text{spad}}(\omega)} \\ &= \frac{D_1 + D_2}{R_b + (1 + \omega^2 C_b^2 R_b^2)(R_s + R_d) + \omega^2 R_d^2 C_d^2 (\omega^2 C_b^2 R_s R_b^2 + R_s + R_b)}, \end{aligned} \quad (6)$$

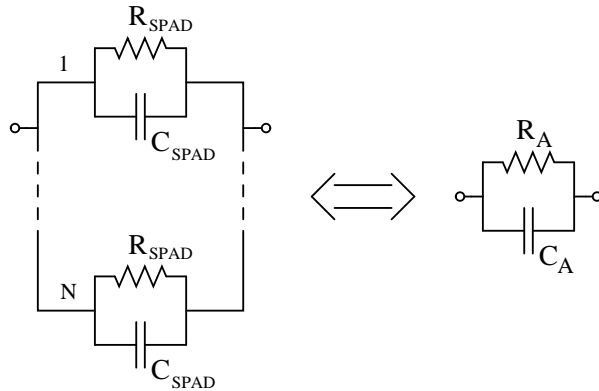


Fig. 12. SIJD model for a SiPM device consisting of  $N$  SPAD devices connected in parallel:  $C_{\text{spad}}$  and  $R_{\text{spad}}$  are, respectively, the capacitance and resistance of the equivalent circuit of a SPAD cell (Fig 11),  $C_A$  and  $R_A$  those of the SiPM device.

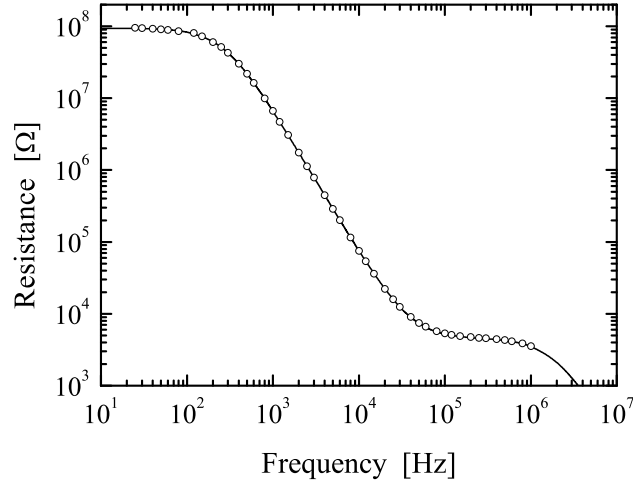


Fig. 13. Measured resistance ( $\circ$ ),  $R_A$ , (in  $\Omega$ ) as a function of frequency (in Hz) with superimposed the continuous line obtained from Eq. (8).

where  $D_1$  and  $D_2$  are

$$D_1 = \omega^2 R_b^2 C_b^2 (R_s + R_d)^2 + \omega^2 R_d^2 C_d^2 (R_s + R_b)^2$$

$$D_2 = (R_d + R_b + R_s)^2 + \omega^2 R_d^2 R_b^2 C_d C_b (2 + \omega^2 R_s^2 C_d C_b).$$

The equivalent electrical circuit\* of a SiPM is shown in Fig. 12. Assuming that each SPAD cell has the same admittance, one finds that the overall admittance of an array is determined by:

$$\begin{aligned} Y_A(\omega) &= N Y_{\text{spad}}(\omega) \\ &= G_A(\omega) + j B_A(\omega) \\ &= \frac{1}{R_A} + j \omega C_A \end{aligned} \quad (7)$$

with

$$G_A(\omega) = \frac{N}{R_{\text{spad}}} \quad (8)$$

$$B_A(\omega) = \omega N C_{\text{spad}}, \quad (9)$$

\*It has to be remarked that one can also add a series resistance to  $R_A$ . This was the case for another SiPM device with 3600 SPAD cells manufactured by STMicroelectronics; for such a device a small additional series resistance of about 1 k $\Omega$  was needed.

Table 2.  $C_d$ ,  $R_d$ ,  $C_b$ ,  $R_b$  and  $R_s$  obtained from a fit of the SIJD model (adapted to a SiPM) to experimental data with the device operated at a reverse bias voltage of 5 V.

$V_r$ [V]	$C_d$ [pF]	$R_d$ [G $\Omega$ ]	$C_b$ [pF]	$R_b$ [M $\Omega$ ]	$R_s$ [k $\Omega$ ]
5	0.262	385	0.056	12.5	195

where  $C_{\text{spad}}$  and  $R_{\text{spad}}$  are obtained from Eqs. (5, 6), respectively; finally,  $N = 64 \times 64 = 4096$  for the present device.

In Fig. 2 (13), the measured values of the capacitance (resistance) are shown as a function of test frequency up to 1 MHz, while the continuous line is that obtained using Eq. (9) [Eq. (8)]. These measurements were carried out at room temperature using the LCR meter with the SiPM device operated at a reverse bias voltage of 5 V. Furthermore, in Table 2 the values of  $C_d$ ,  $R_d$ ,  $C_b$ ,  $R_b$  and  $R_s$  obtained from such a fit of the SIJD model (adapted to a SiPM) to experimental data are reported. It can be remarked that the value obtained for  $R_s$  is in agreement with one of those typically used in the current technology.

Finally, one can point out that the frequency dependence of the present SIJD model<sup>||</sup> for SiPM and photodiode devices is well in agreement with measurements.

#### 4. Conclusions

The electrical characteristics of SiPM devices were investigated as a function of applied reverse bias voltage ( $V_r$ ) and temperature from 410 down to 100 K. The capacitance response was also studied as a function of test frequency. One finds that the measured capacitance decreases i) with increasing the test frequency above 10 kHz at 300 K and ii) with the decreasing of the temperature. Furthermore, the measurement of the leakage current allowed one to determine the value (and its temperature dependence) of the threshold voltage ( $V_{\text{th}}$ ) above which a SiPM begins to operate in Geiger mode:  $V_{\text{th}}$  decreases with lowering temperature at the rate of  $\approx -29$  mV/K from 300 down to 100 K.

It was developed an electrical model to treat the frequency dependence of a SiPM device operated under reverse bias voltage. This model is based on the so-called small-signal ac impedance of junction diode (SIJD) used

<sup>||</sup>The reader can found modelizations of SiPM devices adapted for a time based readout<sup>11</sup> or physical parameters measured at fixed frequencies (e.g., at 100 kHz in Ref.<sup>5</sup> and 1 MHz in Ref.<sup>12</sup>).

for radiation detectors and photodiodes. The model was found to be well suited to account for the SiPM dependencies of capacitance and resistance on frequency.

## References

1. V.D. Kovaltchouk et al., *Nucl. Instr. and Meth. in Phys. Res. A* 538 (2005), 408–415.
2. M. Mazzillo et al., *Nucl. Instr. and Meth. in Phys. Res. A* 591 (2008), 367–373.
3. F. Zappa et al., *Sens. Actuat. A* 140 (2007), 103–112.
4. M. Mazzillo et al., *Sens. Actuat. A* 138 (2007), 306–312.
5. G. Condorelli et al., *Nucl. Instr. and Meth. in Phys. Res. A* 654 (2011), 127–134.
6. C.H. Champness, *J. of App. Phys.* 62 (1987), 917.
7. C. Leroy and P.G. Rancoita, Particle Interaction and Displacement Damage in Silicon Devices operated in Radiation Environments, *Rep. Prog. in Phys.* 70 (2007), 403–625, doi: 10.1088/0034-4885/70/4/R01.
8. C. Leroy and P.G. Rancoita, Principles of Radiation Interaction in Matter and Detection - 3rd Edition - (2011), World Scientific, Singapore, ISBN-978-981-4360-51-7.
9. R.B. Fair, *J. Electrochem. Soc.: Solid State Sci.*, 118 (1971), 971.
10. Wolf, H.F. (1971). Semiconductors Wiley-Interscience, New York.
11. P. Jarron et al., *IEEE Nuclear Science Symposium Conference Record (NSS/MIC)* (2009), 1212–1219, doi: 10.1109/NSSMIC.2009.5402391.
12. F. Corsi et al., *Nucl. Instr. and Meth. in Phys. Res. A* 572 (2007), 416.